Experimental and Numerical Investigation of the Kinematic Theory of Unsteady Separation

M. WELDON[1], T. PEACOCK[1], G. B. JACOBS[2], M. HELU[1], AND G. HALLER[1]

[1]Department of Mechanical Engineering, Massachusetts Institute of Technology, 77 Massachusetts Ave., Rm 1-310, Cambridge, MA 02139, USA

tomp@mit.edu

[2]Department of Aerospace Engineering & Engineering Mechanics, San Diego State University, 5500 Campanile Drive, San Diego, CA 92182, USA

(Received December 13^{th} 2007 and in revised form ??)

We present the results of a combined experimental and numerical study of flow separation in the unsteady, two-dimensional, rotor-oscillator flow. Experimentally-detected material spikes are directly compared to separation profiles predicted from numerical shear-stress and pressure data, using a recent kinematic theory of unsteady separation. For steady, periodic, quasi-periodic and random forcing, fixed separation is observed, and experimental observations and theoretical predictions are in close agreement. The transition from fixed to moving separation is also reported.

---

1. Introduction

Prandtl (1904) initiated the idea that in steady two-dimensional flow, laminar boundary-layer separation occurs at a point of zero skin-friction and negative skin-friction gradient

on a no-slip boundary. He stated that at this point "a fluid-sheet projects itself into the free flow and effects a complete alteration of the motion." If the x-axis is tangent and the y-axis normal to the boundary (cf. figure 1), then Prandtl's steady theory predicts boundary-layer separation at the (x, y) point $\mathbf{p} = (\gamma, 0)$ satisfying:

$$\tau(\gamma) = 0, \quad \tau_x(\gamma) < 0, \tag{1.1}$$

where $\tau(x) = \mu u_y(x, 0)$ is the skin-friction, $(u(x, y), v(x, y))$ the two-dimensional velocity field, and μ the dynamic viscosity.

More generally, the criterion (1.1) applies to flow separation of any scale, i.e., in any situation where a fluid-sheet projects itself into an incompressible and steady mean flow. Examples other than boundary-layer separation include: separating streamlines in Stokes flows, such as Moffatt corner-eddies (Moffatt 1964) and the rotor-oscillator flow (Hackborn, Ulucakli & Yuster 1997); and small-scale separation structures within a boundary layer, such as a separation bubble (Horton 1968). In all these cases, fluid particles separating away from the boundary form a material spike with some spatial scale. The separating streamline (which is the backbone of the material spike) makes an angle α with the wall that can be determined from the skin-friction gradient, τ_x, and wall-pressure gradient, p_x, (Lighthill 1963) using

$$\alpha = \tan^{-1}\left(\frac{-3\tau_x(\gamma)}{p_x(\gamma, 0)}\right). \tag{1.2}$$

For unsteady flows, different definitions of separation can be given (Haller 2004). We follow the lead of Prandtl (1904) and use the term 'separation' to mean the sudden ejection of fluid particles from a rigid boundary in the form of a sharp material spike. While in steady flows a material spike has a clear signature in the skin-friction field, in unsteady flows a material spike does not necessarily have a clear connection with instantaneous Eulerian quantities. As theoretical, numerical and laboratory experiments

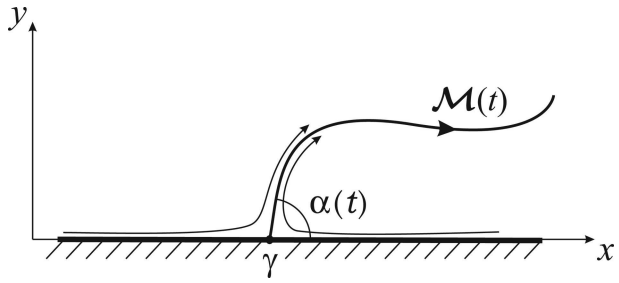

FIGURE 1. A time-dependent unstable manifold $\mathcal{M}(t)$ originating from the fixed separation point $\mathbf{p} = (\gamma, 0)$ making angle $\alpha(t)$ with a no-slip boundary.

reveal, instantaneously-vanishing skin-friction and accompanying flow reversal do not, in general, denote separation in any meaningful sense in unsteady flow (Sears & Telionis 1975), a fact further emphasized by the results of the present study.

Establishing a practical and widely accepted criterion for detecting unsteady separation in experimental fluid flows has proven challenging. Two recent approaches have been the Moore-Rott-Sears (MRS) principle (Sears & Telionis 1975) and a Lagrangian formulation of material-spike formation in boundary-layer equations by Van Dommelen & Shen (1982); for more details see Haller (2004). Among other practical shortcomings, however, the MRS principle still features instantaneous Eulerian quantities, whereas the approach of Van Dommelen is inapplicable to physical, two-dimensional Navier-Stokes flows, which do not exhibit singularities at flow separation (Liu & Wan 1985). Thus, while these two approaches have been highly influential, neither has proven applicable in practical situations.

For near-steady, time-periodic incompressible flows, Shariff, Pilliam & Ottino (1991) and Yuster & Hackborn (1997) showed mathematically and numerically that vanishing, time-averaged skin-friction is a rigorous criterion for material-spike formation on a no-slip boundary. Building on this, Haller (2004) and Kilic, Haller & Neishtadt (2005) developed a general kinematic theory of unsteady separation for two-dimensional flows

with arbitrary time dependence. The theory states that in any mass-conserving flow, a fixed, wall-based material spike forms where the weighted time-averages of the skin-friction and its gradient are zero and negative, respectively. In the incompressible case, the theory agrees with (1.1) for steady flows, and with the results of Shariff, Pilliam & Ottino (1991) and Yuster & Hackborn (1997) for near-steady time-periodic flows.

Here, we present a combined experimental and numerical investigation of the two-dimensional kinematic theory of separation. The system we investigate is the unsteady, rotor-oscillator flow (Hackborn, Ulucakli & Yuster 1997). To the best of our knowledge, this is the simplest experimental arrangement in which one can generate and manipulate unsteady separation under a diverse set of flow conditions. In section 2, we summarize the underlying kinematic theory, before describing our experimental and numerical methods in section 3. We present results for several pertinent unsteady flows in section 4, before drawing our conclusions in section 5.

2. The kinematic theory of fixed separation

The kinematic theory of fixed separation seeks to identify the location and shape of wall-based material spikes from on-wall measurements of flow quantities. In nonlinear dynamical systems theory, the material spikes are signatures of unstable manifolds, i.e., distinguished, time-dependent material lines that shrink to a single boundary point, the separation point, in backward time (figure 1). In forward time, these unstable manifolds collect and eject particles from the vicinity of the wall, thereby creating the familiar material spikes observed at separation points in experimental flow visualizations.

If the flow is unsteady, one might expect material spikes to have time-varying locations. For flows with a well-defined steady mean, however, the separation point is shown to be fixed (Haller, 2004; Kilic, Haller & Neishtadt, 2005), even though the separation spike

deforms in time. If, in addition, the flow is incompressible, then at time t_0 all fixed separation points $\mathbf{p} = (\gamma, 0)$ satisfy

$$\lim_{T\to+\infty} \frac{1}{T} \int_{t_0-T}^{t_0} \tau(\gamma, t)\ dt = 0, \qquad \lim_{T\to+\infty} \frac{1}{T} \int_{t_0-T}^{t_0} \tau_x(\gamma, t)\ dt < 0. \tag{2.1}$$

That is to say, fixed separation occurs at locations where the backward-time average of the skin-friction is zero and the time average of the skin-friction gradient is negative. The first condition in (2.1) is also satisfied at attachment points, i.e., at points that behave like separation points in backward time. The second condition distinguishes $\mathbf{p}$ from an attachment point and excludes flows at rest, ensuring fluid-particle ejection. For steady incompressible flows, (2.1) simplifies to the original Prandtl criterion (1.1).

The time-dependent orientation of the unstable manifold that defines the material spike can also be calculated from distributed skin-friction and wall-pressure measurements. Specifically, the separation angle α at time t_0 satisfies

$$\tan\alpha(t_0) = \frac{\lim_{T\to-\infty} -3\frac{1}{T} \int_{t_0}^{T} \tau_x(\gamma, t)\ dt}{\lim_{T\to-\infty} \frac{1}{T} \int_{t_0}^{T} \left[p_x(\gamma, 0, t) + 3\tau_x(\gamma, t) \int_{t_0}^{t} (1/\mu)\tau(\gamma, s)ds \right] dt}. \tag{2.2}$$

In the limit of a steady flow, this formula reduces to (1.2). The criteria (2.1) and (2.2) can be generalized to any compressible fluid flow that is locally mass-conserving at the point of separation (Haller, 2004), including three-dimensional flows (Surana *et al*, 2007). Additional relations also exist for calculating higher derivatives of the separation profile.

3. Methods

3.1. *Experimental apparatus*

The experimental arrangement utilized was the rotor-oscillator configuration (Hackborn, Ulucakli & Yuster 1997). The experiment, sketched in figure 2, comprised an acrylic tank 40.2 cm long, 8.8 cm wide and 12.0 cm deep. The tank stood in an aluminum support

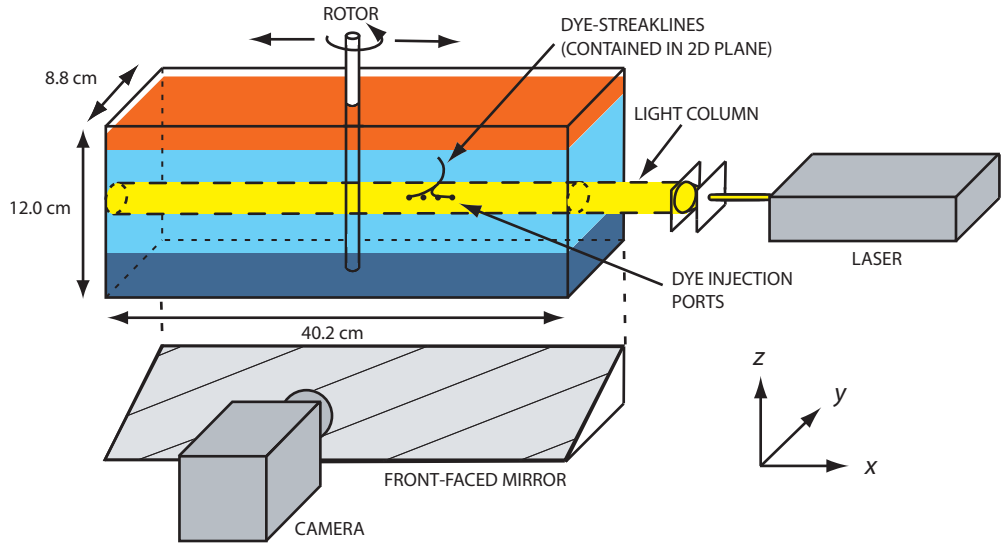

FIGURE 2. Schematic of the experimental apparatus.

frame with leveling mounts and had an open top. An acrylic cylinder of diameter 6.39 mm was held vertically in the tank, at a distance of 26.20 mm from the center of the cylinder to the 40.2 cm-long front wall. The cylinder extended to within 1.0 cm of the bottom of the tank and was mounted to a stepper motor that provided rotation. The alignment of the cylinder was true to the axis of rotation to within 0.13 mm. The stepper motor was, in turn, mounted on a computer-controlled horizontal translation stage, aligned parallel to the front wall so that the cylinder could be moved side-to-side in the tank. Fluid motion was thus driven by a combination of cylinder rotation and translation.

A tri-layer fluid arrangement was used, comprising a 2.8 cm-thick bottom layer of FC-40 Fluorinert electronic coolant, a 5.0 cm-thick center layer of glycerol (in which the visualization took place), and a 1 cm-thick top layer of vegetable oil. The bottom layer of FC-40 suppressed three-dimensional effects caused by interaction between the cylinder and the bottom wall. FC-40 was chosen due to its high density, 1900 kg/m^3, and low viscosity, 2×10^{-6} m^2/s, relative to the working fluid, glycerol, which has a density of 1262 kg/m^3 and a kinematic viscosity of 9×10^{-4} m^2/s. The top layer of vegetable oil

isolated the hydrophilic glycerol from air, where it otherwise readily absorbed moisture, resulting in convection.

Separation was visualized using streaklines created by the laser-induced fluorescence of a neutrally-buoyant dye, mechanically injected through four injection ports in the 40.2 cm-long front wall at the mid-depth of the tank (see figure 2). The injection ports were evenly spaced at 1.33 cm apart, had an exit diameter of 0.56 mm, and were supplied with dye by a syringe pump at a rate of 1 ml/hour. The dye was a mixture of glycerol and fluorescein, for which the concentration of fluorescein was extremely small so as not to noticeably affect the density. Motion of the dye was within a two-dimensional plane at the mid-depth of the tank, to the extent that over the course of an experiment ($\sim$10 mins) there was no detectable vertical motion of the dyed fluid. In each experiment, the arrangement was configured so that dye was injected at points several millimeters away from the separation location, so as not to affect the flow in the region of separation. The resulting location of the injection ports was typically 20-50 mm from the mean rotor x-location.

The evolution of the dyed-fluid in the horizontal plane was recorded using a CCD camera via a 45° front-faced mirror placed beneath the tank. The region of fluid near the wall was illuminated with a 490 nm-wavelength laser-light column to excite the fluorescein molecules. The camera lens was fitted with a 532 nm band-pass filter which allowed only the light emitted by the excited fluorescent molecules to be recorded by the CCD camera. To account for parallax, the camera was calibrated by imaging a ruler placed in the horizontal plane of dye-injection prior to the start of the experiment. Image acquisition was triggered by the rotor-oscillator motion-control system, allowing each image to be matched precisely with a time step of the numerical simulation.

3.2. *Numerical Simulations*

The flow field was computed using FLUENT's incompressible solver with a dynamic mesh. In the computations, the cylinder was used as the point of reference rather than the tank walls, resulting in the four tank walls oscillating while the rotating cylinder was fixed. This allowed a fixed, boundary-fitted mesh around the cylinder, while the dynamic region of the mesh was orthogonal near the straight-sided tanks walls. The orthogonal dynamic region of the mesh facilitated an easy and accurate computational implementation, and was computationally more efficient than the tank reference frame. In the cylinder reference frame, a time-dependent forcing term appeared in the Navier-Stokes equations (Fumagalli 2002). A convergence study was performed to establish a grid-independent solution for a grid with sixty-eight thousand grid points. To further validate the computation, the numerical and experimental streaklines were directly compared. Skin-friction and pressure gradient profiles were extracted from the numerical flow field. The predictions for the separation location and the angle of separation were subsequently calculated from these numerical quantities, and compared with experimental visualizations.

4. Results

4.1. *Steady Forcing*

Steady flow separation was investigated first to validate experiment, simulation and theory. The cylinder rotation rate was set at 20.89 rad/s (199.5 RPM), with no side-to-side cylinder oscillation, resulting in steady flow. The Reynolds number, based on the cylinder diameter, circumferential velocity of the cylinder, and kinematic viscosity of the glycerol, was 0.47. Figure 3(a) shows the separation spike visualized using experimental streaklines (fluorescent green dye). Superimposed on this image are numerical streamlines (which are the same as streaklines in a steady flow) generated from the velocity field of the numerical

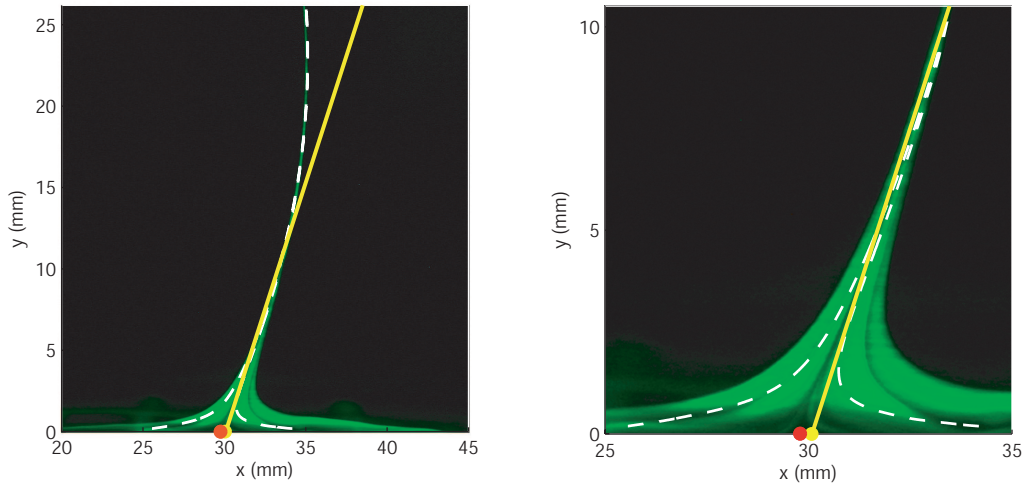

(a) (b)

FIGURE 3. (a) The separating material spike in steady flow. (b) Zoom-in of the material spike in (a). Superimposed on the images are numerical streamlines (white dashed lines), the experimental separation location (red circle), and the predicted separation profile (yellow line) originating from the predicted separation location (yellow circle).

simulation. The numerical streamlines closely follow the experimental streaklines, from the vicinity of the boundary all the way into the body of the fluid. Also superimposed is the predicted separation profile determined using (2.1) and (2.2).

The experimental point of separation was determined in this, and later, studies by observing the location of the dye-free region within the separation spike, near the wall. This region, which can be more clearly seen in figure 3(b), contains the marginally-stable fixed point to which fluid particles are drawn, before being ejected away from the wall. The location of the separation point was defined by tracing the trajectory of the dye-free region at the center of the spike back to the wall. The experimental error was defined to be the width of the dye-free region 0.5 mm away from the wall. The location of the numerical zero-skin-friction point matches the experimentally-determined separation

point to better than 0.5 mm. The linear prediction of the separation angle also captures the near-wall geometry of the separation spike by lining up with the dye-free region within the spike. Far from the wall, the linear approximation deviates from the experimental spike, which is to be expected given the wall-based approach.

4.2. *Periodic Forcing*

Periodic, unsteady flows were generated by combining cylinder rotation at 20.89 rad/s with side-to-side sinusoidal oscillation. The period of oscillation was six seconds. Five peak-to-peak displacements were investigated, ranging from 8 mm to 40 mm in 8 mm incremental steps. In all experiments, the separation location remained fixed over the entire period of oscillation, while the angle of the separation profile with respect to the wall oscillated. The persistence of a fixed separation location was particularly dramatic for the largest amplitude oscillations, for which the cylinder moved up to four times the width of the domain shown in figure 3(b). The periodicity of the flow was verified by identifying that the material spike was precisely repeated at the same phase over many cycles of oscillation.

The experimental separation location and orientation could again be determined by observing a dye-free region at the heart of the material spike. For the different amplitudes of oscillation, the experimental location was compared with the numerical prediction calculated using (2.1). The results, including the steady case, are shown in figure 4(a). For each case, the location of the time-average zero-skin-friction point closely matches the experimental separation location. The error bars have a bias since the dye-free region is asymmetric; the fluid velocity to the left of the separation location is much larger than the fluid velocity to the right, driving fluid particles closer to the separation point before they are ejected away from the wall.

The results in figure 4 show that the amplitude of oscillation had a significant effect

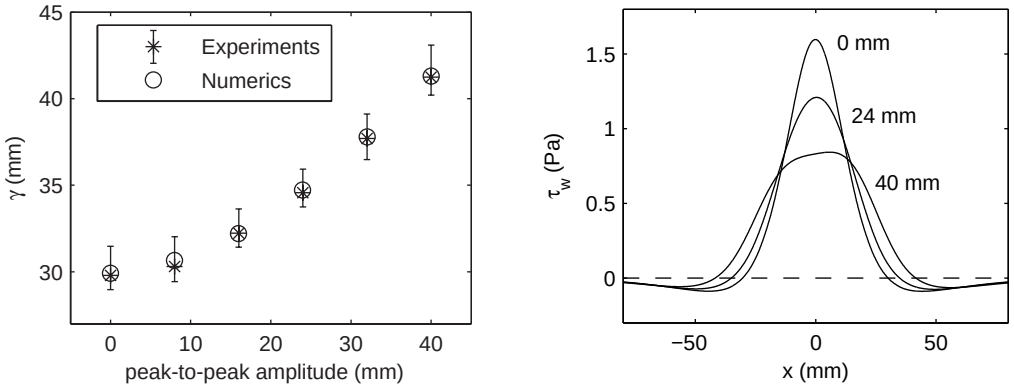

(a) (b)

FIGURE 4. (a) Comparison of the experimental and numerical separation location, γ, for periodic forcing. (b) Mean skin-friction profiles for 0 mm, 24 mm, and 40 mm peak-to-peak amplitude oscillations. Where the profiles cross the dashed line identifies points of zero mean skin-friction.

on the separation location relative to the mean rotor location, $x = 0$. The velocity field induced by both cylinder rotation and oscillation changes dramatically over the period of an oscillation and with increasing amplitude of oscillation; so too, therefore, does the instantaneous skin-friction profile. This, in turn, leads to very different time-average skin-friction profiles for the different amplitudes of oscillation, as shown in Figure 4(b), for which the location of the $+x$ zero-crossing increases with increasing amplitude of oscillation. It should be noted that the $+x$ zero-crossing represents a separation point and is distinguished from the $-x$ zero-crossing reattachment point by the second condition in (2.1).

The kinematic approach performed very well in determining the angle of separation. As an example, in figure 5 we compare the material spike orientation with the predictions of (2.2) for a 24 mm oscillation amplitude. The results for this intermediate case are shown at three instances: (a) the minimum separation angle ($\sim 60°$), occurring 2.0 s into the 6.0 s period oscillation, (b) an intermediate separation angle ($\sim 71°$), occurring after

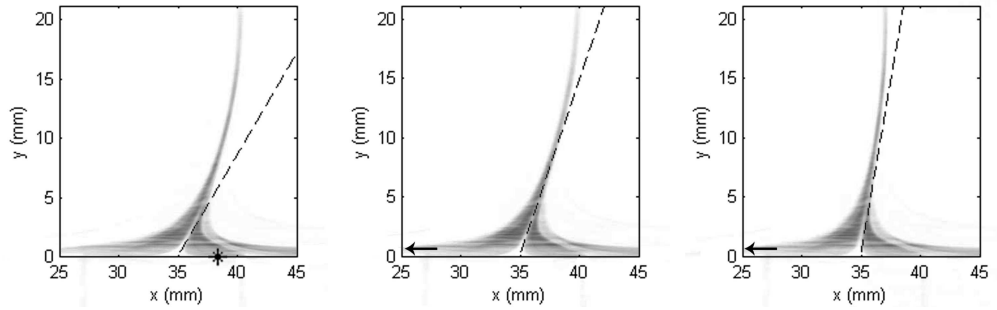

(a) (b) (c)

FIGURE 5. Separating material spike in periodic flow (24 mm peak-to-peak oscillation amplitude) compared with the numerical prediction (dashed line) for: (a) minimum separation angle (t=2.0 s); (b) intermediate separation angle (t=3.7 s); (c) maximum angle (t=5.0 s). (∗) or (←) indicates the location of the instantaneous zero skin-friction point.

3.7 s, and (c) the maximum separation angle ($\sim 80°$), occurring after 5.0 s. In all cases, the theoretical time-dependent linear profile predicted using (2.1) and (2.2) leaves the wall at the same angle as does the experimental dye-free region. When the curvature of the experimental spike is small (figures 5(b) and (c)), which was typical for the smaller amplitudes of oscillation we investigated, the linear profile follows the separation spike well into the fluid. When there is significant curvature of the spike (figure 5(a)), the shape of the experimental spike and the linear prediction diverge within a few mm of the wall, though the wall prediction of the separation location remains valid.

Finally, an important point to raise is the location of the instantaneous zero-skin-friction point during these experiments. Its location for the 24 mm oscillations is indicated in figure 5 using (∗) for the exact location or (←) to point to it, if it falls outside the field of view, which is often the case. It is thus clear that the location of the instantaneous zero-skin-friction point does not provide a reliable indicator of the location of separation for these experiments.

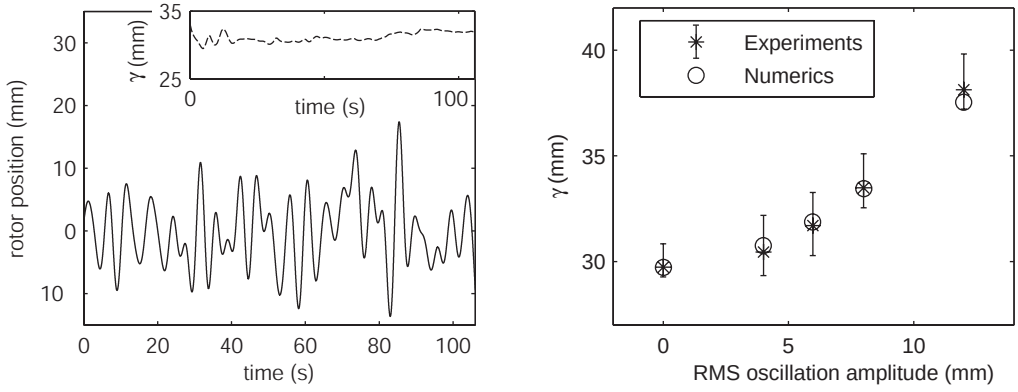

(a) (b)

FIGURE 6. (a) 5.97 mm RMS amplitude quasi-periodic rotor location (main plot line) and convergence of the fixed separation location, γ (inset); (b) the fixed separation location, γ, as a function of the RMS amplitude of oscillation for quasi-periodic forcing.

4.3. *Quasi-Periodic and Random Forcing*

Quasi-periodic forcing was applied by rotating the cylinder at 20.89 rad/s, while translating it laterally with a complex quasi-periodic motion, designed to emulate random forcing. Each signal had a zero mean, and comprised twenty incommensurate frequencies with random phase and a common amplitude. One example of a signal used, having a 5.97 mm RMS amplitude, is presented in the lower part of figure 6(a).

A fixed experimental separation point was observed for all the quasi-periodic cases studied, and its location matched numerical predictions to within 1 mm for oscillations of RMS amplitudes up to 12 mm (peak-to-peak amplitudes of over 80 mm), as shown in figure 6(b). Again, the persistence of a fixed separation spike under such dramatically varying flow conditions was striking. It is noted, however, that (2.1) and (2.2) formally require a time-history approaching $-\infty$ to converge to a fixed separation point for general unsteady flows; in practice, one therefore needs a sufficiently long time-history to obtain reasonable convergence. In the upper part of figure 6(a), the convergence of (2.1) is

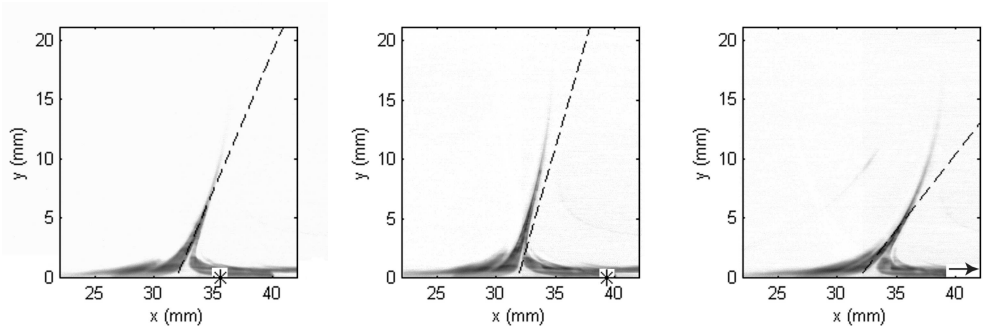

(a) (b) (c)

FIGURE 7. Separation spike in 5.97 mm RMS quasi-periodic flow compared with the numerical prediction for: (a) an intermediate angle (t=52.3 s); (b) a large angle (t=73.0 s); (c) a small angle (t=79.0 s). (∗) or (→) indicates the location of the instantaneous zero-skin-friction point.

plotted for the forcing shown in the lower part of the same figure. Near convergence (within several mm) was achieved within 20 s, but an additional 50 s was required to converge to within 1 mm. This error is of similar magnitude to the discrepancy between the experiment and numerical separation location in figure 6(b). We also found that the prediction was sensitive to anomalously large changes in cylinder position in the quasi-periodic signal, which could take many tens of seconds to average out.

The prediction of the experimental separation angle converged much faster than the prediction of the separation position, as the criterion (2.2) is more heavily biased to recent events. The structure of the integral in the denominator of (2.2) repeatedly integrates over recent wall-shear history, and this term dominates the equation. In figure 7, the numerical predictions are compared with experimental visualizations for the 5.97 mm RMS signal. The separation location and angle are visualized at three instances: (a) an intermediate angle (66°) at time $t = 52.3$ s, (b) a large angle (74°) at time $t = 73.0$ s, and (c) a small angle (50°) at time $t = 79.0$ s. As with the periodic case, the angle

is generally very well predicted; although, when the curvature of the spike is large, the linear profile captures the separation geometry within only the first few mm of the wall.

Finally, experiments were performed in which motion of the cylinder was indeed random with a zero mean amplitude. The system was studied for RMS oscillation amplitudes up to 10 mm (peak-to-peak over 60 mm), constrained only by the capability of the translation stage. The resulting cylinder motion was qualitatively very similar to that presented in figure 6(a). We saw no qualitative difference in the system behavior for this scenario; the material spike still originated from a fixed location, despite the strongly-varying external flow field, and appeared just as in figure 7. We do not have direct comparison between experiments and numerics in this regime, however, because of technical challenges in specifying random forcing in FLUENT.

5. Discussion & Conclusions

We have performed a combined experimental and numerical study of the kinematics of a separating material spike in the unsteady, rotor-oscillator flow. Under a wide variety of flow conditions fixed separation was observed, the location and orientation of which was accurately predicted using a recently-developed, kinematic theory of unsteady separation. These results further emphasize that knowing the instantaneous value of Eulerian quantities, such as skin-friction and surface-pressure, is generally insufficient for identifying the location of a separating material spike. Rather, one must record and appropriately average a time-history of such quantities.

While this study investigated some exciting new ideas, much remains to be understood. There are interesting cases for which the observed separation location is different from those predicted by criteria (2.1) and (2.2). One example is very slow side-to-side motion of the cylinder, which approaches a quasi-steady state. For periodic forcing, we found

that as the oscillation frequency was reduced the location of the material spike started to oscillate until, at very low frequencies, the material spike followed the cylinder motion precisely. While, in principle, the base of the separating material spike was still attached to the wall at a fixed point (Haller, 2004), in practice this region was so indistinguishably small it could not be resolved; instead, the body of the material spike appeared to follow the motion of the instantaneous zero-skin-friction point.

We investigated another scenario in which the amplitude of oscillation was significantly increased. In this case the material spike was dragged side-to-side and no longer retained a nicely-formed shape. Instead, it became quite deformed, and it was practically difficult to identify a separation location. We note that if the oscillations were made arbitrarily large, then the cylinder would spend so little time at any given location we would not expect to see a material spike on a length scale that could be experimentally detected; although one may exist on a much smaller, undetectable scale.

The next challenge is to extend the kinematic separation approach to unsteady flows with arbitrary time-dependence, and be able to recognize the creation and/or breakdown of moving material spikes using surface data. Criteria must be developed that balance the time required for a fluid element to be ejected a certain distance from the boundary with the characteristic unsteady time-scale of the flow. Such results have recently been obtained by Surana & Haller (2007) for two-dimensional flows with an unsteady mean component whose variation is slower than those of the oscillations imposed on the mean.

Further generalization and extension of these results is a challenging problem indeed, but the inherent difficulty of such a task should not detract from the significant progress in the current study. Primarily, we have rigorously and successfully tested a new criterion for detecting fixed separation in unsteady flows; and, perhaps most remarkably, we have

demonstrated that fixed separation can occur even in a random experimental flow field, which is kinematically equivalent to the conditions within a turbulent boundary layer.

REFERENCES

Fumagalli, M. 2002 *A numerical investigation of particle motion and deposition on a cross oscillating cylinder.* MS Thesis, University of Illinois at Chicago, Chicago, IL.

Haller, G. 2004 Exact theory of unsteady separation for two-dimensional flows. *J. Fluid Mech.* **512**, pp. 257-311.

Hackborn, W. W., Ulucakli, M. E., & Yuster, T. 1997 A theoretical and experimental study of hyperbolic and degenerate mixing regions in a chaotic Stokes flow. *J. Fluid Mech.* **346**, pp. 23-48.

Horton, H. P. 1968 *Laminar separation bubble in two- and three-dimensional incompressible flow.* Ph.D. thesis, University of London.

Kilic, M. S., Haller, G., and Neishtadt, A. 2005 Unsteady fluid slow separation by the method of averaging. *Phys. Fluids* **17**, 067104

Lighthill, M. J. 1963 Boundary Layer Theory. In *Laminar Boundary Layers* (ed. L. Rosenhead). Dover.

Liu, C. S. & Wan, Y.-H. 1985 A simple exact solution of the Prandtl boundary layer equations containing a point of separation. *Arch. Rat. Mech. Anal.* **89**, pp. 177-185.

Moffatt, H. K. 1964 Viscous and Resistive Eddies Near a Sharp Corner. *J. Fluid Mech.* **18**, pp. 1-18.

Prandtl, L. 1904 Über Flüssigkeitsbewegung bei sehr kleiner Reibung. *Verh. III, Int. Math. Kongr., Heidelberg* pp. 484-491.

Sears, W. R. & Telionis, D. P. 1975 Boundary-layer separation in unsteady flow. *SIAM J. Appl. Maths* **28** pp. 215-235.

Shariff, K., Pulliam, T. H., & Ottino, J. M. 1991 A dynamical systems analysis of kinematics in the time-periodic wake of a circular cylinder. *Lect. Appl. Math.* **28**, pp. 613-646.

Surana, A., & Haller, G., Ghost manifolds in slow-fast systems, with an application to unsteady fluid flow separation. *Physica D*, to appear.

Surana, A., Jacobs, G., Grunberg, O. & Haller, G., Exact theory of fixed unsteady separation in three-dimensional flows, *Phys. Fluids*, to appear

Van Dommelen, L. L. & Shen, S. F. 1982 The genesis of separation. In *Numerical and Physical Aspects of Aerodynamics Flow* (ed. T. Cebici) pp. 283-311. Long Beach, California.

Yuster, T. & Hackborn, W. W. 1997 On invariant manifolds attached to oscillating boundaries of Stokes flows. *Chaos* **7**, pp. 769-776.